Spectroscopic Studies of Zinc(II)- and Cobalt(II)-Associated *Escherichia coli* Formamidopyrimidine−DNA Glycosylase: Extended X-ray Absorption Fine Structure Evidence for a Metal-Binding Domain†

Garry W. Buchko,‡ Nancy J. Hess,§ Viswanath Bandaru,‡ Susan S. Wallace,‡ and Michael A. Kennedy*,§

Department of Microbiology and Molecular Genetics, University of Vermont, Burlington, Vermont 05405, and Environmental Molecular Sciences Laboratory and Biogeochemistry Resources, Pacific Northwest National Laboratories, Richland, Washington 99352

Received June 15, 2000

ABSTRACT: Formamidopyrimidine−DNA glycosylase (Fpg) is a 30.2 kDa protein that plays an important role in the base excision repair of oxidatively damaged DNA in *Escherichia coli*. Sequence analysis and genetic evidence suggest that zinc is associated with a C4-type motif, C_{244}-X_2-C_{247}-X_{16}-C_{264}-X_2-C_{267}, located at the C-terminus of the protein. The zinc-associated motif has been shown to be essential for damaged DNA recognition. Extended X-ray absorption fine structure (EXAFS) spectra collected on the zinc-associated protein (ZnFpg) in the lyophilized state and in 10% frozen aqueous glycerol solution show directly that the metal is coordinated to the sulfur atom of four cysteine residues. The average Zn−S bond length is 2.33 ± 0.01 and 2.34 ± 0.01 Å, respectively, in the lyophilized state and in 10% frozen aqueous glycerol solution. Fpg was also expressed in minimal medium supplemented with cobalt nitrate to yield a blue-colored protein that was primarily cobalt-associated (CoFpg). The profiles of the circular dichroism spectra for CoFpg and ZnFpg are identical, suggesting that the substitution of Co^{2+} for Zn^{2+} does not alter the structure of Fpg. A similar conclusion is reached upon the analysis of two-dimensional $^{15}N/^{1}H$ HSQC spectra of uniformly ^{15}N-labeled samples of ZnFpg and CoFpg; the spectra are similar and display features characteristic of a structured protein. Biochemical assays with a 54 nt DNA oligomer containing 7,8-dihydro-8-oxoguanine at a specific location show that CoFpg and ZnFpg are equally active at cleaving the DNA at the site of the oxidized guanine. EXAFS spectra of CoFpg indicate that the cobalt is coordinated to the sulfur atom of four cysteine residues with an average Co−S bond length of 2.28 ± 0.01 and 2.29 ± 0.01 Å, respectively, in the lyophilized state and in 10% frozen aqueous glycerol solution. The structural similarity between CoFpg and ZnFpg suggests that it is biologically relevant to use the paramagnetic properties of Co^{2+} as a structural probe.

DNA is continuously being damaged by oxidation. Such reactions can occur on exposure to exogenous agents such as ionizing radiation and chemicals (*1, 2*). However, the most important source of DNA oxidation is endogenous, a consequence of normal metabolism (*3, 4*). Unrepaired, oxidative DNA lesions may have deleterious cellular consequences, such as cell death, mutagenesis, carcinogenesis, and aging (*5*). A number of repair pathways exist to prevent biological expression of oxidative DNA damage. One mechanism, base excision repair (BER), appears to be responsible for the replacement of most oxidative base damage (*4, 6*−*8*).

One of the BER enzymes identified in *Escherichia coli* is formamidopyrimidine−DNA glycosylase (Fpg),[1] a 269 residue protein with a molecular mass of 30.2 kDa (*9*). Fpg binds double-stranded DNA and performs three catalytic activities in vitro; it is a (i) DNA glycosylase, (ii) AP lyase, and (iii) deoxyribophosphodiesterase. Substrates recognized and released by the DNA glycosylase activity of Fpg include 7,8-dihydro-8-oxoguanine (8-oxoG) (*10, 11*), 2,6-diamino-4-hydroxy-5-formamidopyrimidine (Fapy-G) (*12*), the adenine equivalents 8-oxoA and Fapy-A (*11*), 2,2,4-triaminooxazolone (*13*), 5-hydroxyuracil (*14*), 5-hydroxycytosine, 5,6-dihydrothymine (*14, 15*), and α-(*R*)-hydroxy-*β*-ureidoisobutyric acid (*16*). The AP lyase activity of Fpg functions to

† Part of the research was performed in the Environmental Molecular Sciences Laboratory (a national scientific user facility sponsored by the DOE Biological and Environmental Research) located at Pacific Northwest National Laboratory and operated for DOE by Battelle. The Stanford Synchrotron Radiation Laboratory is funded by Basic Energy Sciences, U.S. Department of Energy. This work was performed under the auspices of the U.S. Department of Energy (Contracts DE-AC06-76RLO1830 to M.A.K. and DE-FG02-98ER 45723 to S.S.W.) and was supported by the Department of Energy Office of Biological and Environmental Research Program under Grant 249311 KP11-01-01. G.W.B. is a visiting scientist from the University of Vermont at Pacific Northwest National Laboratories.

* To whom correspondence should be addressed. Tel.: 509-372-2168; Fax: 509-376-2303; E-mail: ma_kennedy@pnl.gov.

‡ University of Vermont.

§ Pacific Northwest National Laboratories.

[1] Abbreviations: Fpg, formamidopyrimidine−DNA glycosylase; ZnFpg, zinc-associated Fpg; CoFpg, cobalt-associated Fpg; 8-oxoG, 7,8-dihydro-8-oxoguanine; AP, apurinic/apyrimidinic; EXAFS, extended X-ray absorption fine structure; XANES, X-ray absorption near-edge structure; CD, circular dichroism; NMR, nuclear magnetic resonance; HSQC, heteronuclear single quantum coherence; DTT, dithiothreitol; EDTA, ethylenediaminetetraacacetic acid.

10.1021/bi001377k CCC: $19.00
Published on Web 09/14/2000

cleave the DNA backbone 3′ to the abasic site via successive β- and δ-elimination reactions to produce a 3′-phosphate (*17*−*19*). Fpg also possesses a deoxyribophosphodiesterase activity that can remove the 5′-deoxyribose phosphate moiety from an AP site incised by one of the hydrolytic AP endonucleases (*20*). Bacterial strains lacking the *fpg* gene show a mutator phenotype (*21*) that is strongly enhanced by the inactivation of the mutY gene (*22*). When 8-oxoG is bypassed by various DNA polymerases, either dAMP or dCMP can be inserted (*23*). Consequently, if replication occurs prior to 8-oxoG removal, a G to T transversion can occur (*24*−*28*). The mutY gene product is a protein that recognizes and removes the A from 8-oxoG·A mispairs (*29*−*31*), giving Fpg another chance to repair 8-oxoG before a second round of DNA replication occurs. Genes for a functional analogue of Fpg, namely, *Ogg1*, have been cloned from yeast and mammals (*32*−*38*).

Analysis of the amino acid sequence of Fpg suggests the protein contains a C4-type zinc-binding motif, C_{244}-X_2-C_{247}-X_{16}-C_{264}-X_2-C_{267}, located near the carboxyl terminus (*39*). Biochemical and site-directed mutagenesis studies corroborate the sequence analysis predictions, showing that the DNA glycosylase, abasic site nicking, and deoxyribose excising activities of Fpg are reduced when the cysteine residues in the putative metal-binding motif are chemically modified or mutated (*40*). Despite substantial indirect evidence for a C-terminal C4-type metal-binding motif in Fpg (*10, 40*), no direct evidence for such a metal-binding motif has been reported. To directly show that Fpg contains a metal-binding motif and to identify the ligands coordinated to the metal, extended X-ray absorption fine structure (EXAFS) spectra were collected on Fpg samples containing zinc (ZnFpg) and cobalt (CoFpg). Because EXAFS spectroscopy can identify the element at the metal center and provide information on interatomic distances within picometers, the number and type of ligand atoms, and the statistical and/or thermal disorder of the shells of atoms surrounding the metal center (*41, 42*), it has been used to characterize the local structural environment around the metal in a variety of metalloproteins (*43*−*46*). Circular dichroism and NMR data were also collected on ZnFpg and CoFpg to determine if there were any structural differences between the zinc- and cobalt-associated proteins. To compare the DNA glycosylase activity of zinc- and cobalt-associated Fpg, a double-stranded 54 nt DNA oligomer containing a single, site-specific 8-oxoG lesion was synthesized and incubated with various concentrations of ZnFpg and CoFpg. The results are discussed in terms of using the paramagnetic properties of Co^{2+} to probe the structure of Fpg.

EXPERIMENTAL PROCEDURES

Preparation of Fpg Proteins. The DNA coding sequence for the *E. coli* Fpg protein was cloned into the vector pET-11d and transfected into the host *E. coli* bacterial strain BL21(DE3) (Novagen, Inc., Madison, WI). Cells were grown (37 °C) to an OD_{600nm} reading of 0.6−0.8 in 750 mL of minimal medium containing 100 μg/mL ampicillin (Sigma, St. Louis, MO). Following induction with 1.0 mM isopropyl-1-thio-β-D-galactopyranoside (Sigma), the medium was supplemented to a final concentration of 0.01 mM zinc acetate [$Zn(CH_3CO_2)_2 \cdot 2H_2O$] (Sigma) or 0.007 mM cobalt nitrate [$Co(NO_3)_2 \cdot 6H_2O$] (Sigma) and the temperature lowered to 28 °C. After 2−3 h of protein expression, the cells were harvested by centrifugation for 10 min at 5000*g* (4 °C) and resuspended in 40 mL of 50 mM potassium phosphate (Sigma), pH 7.5. Phenylmethylsulfonyl fluoride (Sigma) (0.2 μM) was added to the cell suspension, and the cells were broken by three passes through a French Press (SLM Instruments Inc., Rochester, NY). The debris was sonicated for 1 min and then spun at 17500 rpm for 60 min in a JA-20 rotor in a Beckman Avanti J-25 centrifuge (Palo Alto, CA). Most of the soluble Fpg was precipitated with 12 g of ammonium sulfate (∼50% saturation), pelleted, and resuspended in 40 mL of buffer containing 15 mM potassium phosphate and 2 mM DTT, pH 7.2. Ten to twenty milliliters of the resulting supernatant was applied to a BioRad hydroxyapatite CHT-II cartridge (Hercules, CA) attached to a BioCAD Sprint Perfusion Chromatography System (PerSeptive Biosystems, Framingham, MA). The column was washed with 10 mM potassium phosphate, 1.0 mM DTT, pH 7.1, and eluted with a linear gradient of 0−400 mM potassium phosphate, 1.0 mM DTT, pH 7.1, over 10 column volumes. Fpg eluted as a baseline-resolved peak at approximately 300 mM potassium phosphate. The peak containing Fpg was collected, pooled, and concentrated to 0.5−0.8 mM with a Centriprep-10 (Amicon Inc., Beverly, MA). While the ZnFpg solution was colorless, the CoFpg sample was a blue−green color as is characteristic of cobalt-containing metalloproteins (*47*). Sample purity was greater than 90% as determined by SDS−polyacrylamide gel electrophoresis and Coomassie Blue staining. The final yield of Fpg obtained from the soluble fraction was approximately 15 mg/L for both ZnFpg and CoFpg.

8-OxoG DNA Glycosylase Assay. The 8-oxoG DNA glycosylase activity of Fpg was assayed using a 54 nt double-stranded DNA oligomer containing a single 8-oxoG·C base pair at position 24. The two single-strand 54 nt oligos were synthesized by standard phosphoramidite chemistry using an 8-oxoG phosphoramidite (Glen Research, Sterling, VA) to introduce the modified base into one strand. One picomole of the 8-oxoG-containing oligomer was 5′-end-labeled by mixing 10 μCi of [γ-^{32}P]ATP (6000 Ci/mmol; 10 mCi/mL; NEN Dupont) and 5 units of T4 polynucleotide kinase (New England Biolabs, Beverly, MA) in a final volume of 20 μL and incubating at 37 °C for 30 min. The kinase was heat-inactivated (65 °C for 5 min) and the 8-oxoG-containing strand annealed with 1.5−2-fold molar excess of its complementary strand. The concentration of the 5′-end-labeled duplex DNA was adjusted to 1 fmol/μL in an assay buffer containing 10 mM Tris-HCl, 1.0 mM EDTA, and 50 mM NaCl (pH 8.0). Five femtomoles of the duplex substrate was mixed with 10-fold serial dilutions of the ZnFpg and CoFpg in storage buffer (300 mM potassium phosphate, 1.0 mM DTT, pH 7.2). The reaction mixtures were incubated at 37 °C for 5 min, quenched with 3 μL of formamide buffer (0.05% xylene cyanol, 0.05% bromophenol blue, 10 mM EDTA in 98% formamide), and directly loaded onto a 12% denaturing polyacrylamide gel. The 23 nt DNA oligo cleavage product was visualized by ^{32}P autoradiography.

Circular Dichroism Spectroscopy. Circular dichroism spectra were obtained on a Aviv model 62DS spectropolarimeter calibrated with an aqueous solution of ammonium *d*-(+)-camphorsulfonate. The measurements were obtained on ZnFpg and CoFpg solutions in 300 mM potassium

phosphate, pH 7.2, with and without 10% glycerol (v/v), at 25 °C in a quartz cell of 0.1 mm path length. The samples were of approximately equal concentrations, 0.102 mM (ZnFpg) and 0.088 mM (CoFpg), as determined using the Bradford assay. Each spectrum was the result of averaging two consecutive scans from 250 to 190 nm recorded with a bandwidth of 1.0 nm and a time constant of 1.0 s. Following the appropriate subtraction of a blank spectrum of either water or 10% aqueous glycerol, the data were smoothed with a binomial function. Thermal denaturation curves for both proteins in 300 mM potassium phosphate (no glycerol) were obtained by recording CD spectra at 2.5 °C intervals from 5 to 80 °C at 220 nm. Following acquisition of the thermal denaturation data, the samples were returned to 25 °C, and a full CD spectrum was recorded.

NMR Spectroscopy. NMR samples, ~0.7 mM, of ZnFpg and CoFpg were prepared in 600 μL of 90% H_2O/10%D_2O in the following NMR buffer: 300 mM potassium phosphate, 1.0 mM DTT, 50 μM NaN_3, pH 7.3. Two-dimensional $^{15}N/^{1}H$ HSQC (*48, 49*) or $^{15}N/^{1}H$ HSQC-TROSY (*50*) spectra were collected at 35 °C on Varian 800- or 600-Unityplus spectrometers. A ZnFpg sample was frozen with liquid nitrogen, lyophilized, and resuspended in NMR buffer, and a $^{15}N/^{1}H$ HSQC spectrum was collected immediately afterward.

EXAFS Spectroscopy. The EXAFS data were collected under dedicated operating conditions (3.0 GeV and 40−90 mA current) using synchrotron radiation on Beamline 4-2 and 4-1 at the Stanford Synchrotron Radiation Laboratory. For the lyophilized samples, 10−15 mg of Fpg in ~300 mM potassium phosphate buffer was pressed into a holder (1.5 × 0.25 cm) and sealed with Kapton tape. For the frozen 10% aqueous glycerol samples, 0.9 mM ZnFpg and 0.7 mM CoFpg in ~300 mM potassium phosphate buffer were loaded into a specially designed 125 μL cell holder. Both samples were quickly frozen in liquid nitrogen and then loaded onto a liquid nitrogen cryostat for spectroscopic measurements. Spectra were collected at the Zn and Co K-edge in the fluorescence mode using a multielement germanium detector. In addition, the fluorescence signal of a ZnS standard was measured using a Lytle detector at 300 K. Energy calibration for ZnFpg was made by assigning the first inflection point in the absorption edge of the zinc foil to 9659 eV. The absorption spectrum was normalized by fitting polynomials through the pre- and postedge regions. At E_0, the ionization threshold energy, the value of the extrapolated preedge was set to zero, and the difference between the extrapolations of the pre- and postedge polynomials was set to unity. The energy scale of the data was converted from eV to *k*-space using the relationship: $k = [(2m_e(E - E_0)/\hbar^2]^{1/2}$, where m_e is the electron rest mass and E_0 for the cobalt and zinc K-edges is set at 7714.4 and 9659 eV, respectively.

The EXAFS oscillations were extracted by fitting a polynomial spline function through the postedge region and normalizing the difference between this approximation of the solitary-atom EXAFS and the actual data with the absorption decrease calculated using the parametrized absorption coefficients of McMaster (*51*). The number and position of the nodes in the spline were varied to minimize the integrated intensity in the Fourier transform moduli of the EXAFS between 0 and 2.0 Å. The resulting EXAFS oscillations are defined by the relationship: $\chi(k) = [\mu(k) - \mu_{0,\mathrm{spline}}(k)]/[\Delta\mu_{k=0}\mu_{0,\mathrm{M}}(k)]$, where $\mu(k)$ is the observed absorption, $\mu_{0,\mathrm{spline}}(k)$ is the fitted spline, $\Delta\mu_{k=0}$is the observed absorption coefficient at k=0, and $\mu_{0,\mathrm{M}}(k)$ is the calculated atomic absorption coefficient based on the McMaster tables. Fourier transforms were taken over photoelectron wavevector ranges that varied on the basis of the signal-to-noise ratio for each element. EXAFS nodes were selected as endpoints to the Fourier transform range, and a sine window function was used to dampen the EXAFS oscillations at the endpoints.

The phase and amplitude for the cation−sulfur path were calculated using the ab initio code FEFF7.02 (*52, 53*). The normalized phase and amplitudes of the cation−sulfur scattering paths were used to fit the experimentally measured EXAFS. The ZnS T^2_d structure was used to approximate the metal cation tetrahedral environment in both proteins; for the Co−S scattering path, Co was substituted for Zn in the ZnS standard without modification of the lattice parameters or fractional coordinates. The number of sulfur atoms and the metal−sulfur bond distance were determined using the normalized backscattering amplitude and phase functions from FEFF to fit the experimental EXAFS data using the following equation, which is summed over all backscatterers, *i*:

$$x(k) = \sum_i \frac{N_i S_i F_i(k)}{kR_i^2} \exp(-2k^2\sigma_i^2) \times \exp\left(\frac{-2R_i}{\lambda}\right) \sin(2kR_i + \phi_i(k))$$

N_i is the number of backscattering atoms at a distance R_i from the absorber. S_i is a scale factor with values that usually vary between 0.8 and 1.0 to account for multielectron effects and inelastic scattering not calculated by FEFF7.02 (*52, 53*). Values of the scale factor S_i are typically determined empirically by fitting standards with calculated scattering amplitudes. Any necessary correction between the observed and calculated amplitude is then the assigned value for the scale factor, S_i. This is not a very satisfactory approach because there are many experimental and sample-dependent artifacts that can affect the experimental amplitudes. In this work we have chosen not to apply a correction factor to the FEFF calculated amplitudes for either Zn or Co data; therefore, a S_i value of 1 is used. The quantities $F_i(k)\exp(-2R_i/\lambda)$ and ϕ_i are the backscattering amplitude and phase functions, respectively, that are calculated by FEFF7.02 for each path. σ_i^2 is the Debye−Waller factor and represents the root-mean-squared variation in the absorber−backscatterer interatomic distance.

RESULTS

Glycosylase Activity of ZnFpg and CoFpg. A 54 nt double-stranded DNA oligomer containing a single 8-oxoG·C base pair at position 24 was incubated with various concentrations of Fpg. The major 5′-labeled glycosylase cleavage product, a 23 nt oligo containing a 3′-phosphate, was observed by denaturing polyacrylamide gel electrophoresis. Figure 1 is an autoradiograph of a 12% polyacrylamide gel of the reactions. In the absence of Fpg, only a single band, corresponding to uncleaved DNA substrate, is observed at the top of the gel (lanes 1 and 6). At Fpg concentrations of

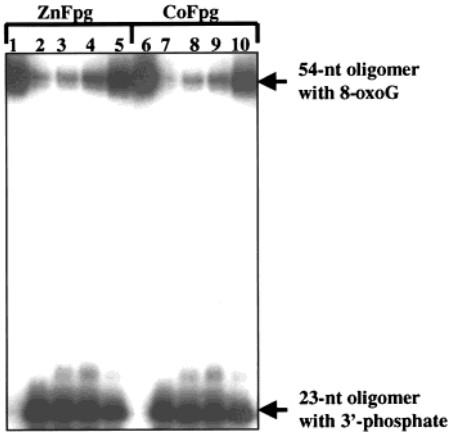

FIGURE 1: Autoradiogram of a 12% polyacrylamide gel comparing the DNA glycosylase activity of ZnFpg and CoFpg. A 5′-^{32}P-labeled 54 nt oligo containing an 8-oxoG·C base pair at position 24 was used as the substrate. The uncut substrate is at the top of the gel while the cleavage product is found at the bottom of the gel; the major band is a 23 nt oligo 3′-phosphate. Lanes 1 and 6, no Fpg; lanes 2 and 7, stock Fpg (0.5 mM); lanes 3 and 8, 0.05 mM Fpg; lanes 4 and 9, 0.005 mM Fpg; lanes 5 and 10, 0.0005 mM Fpg.

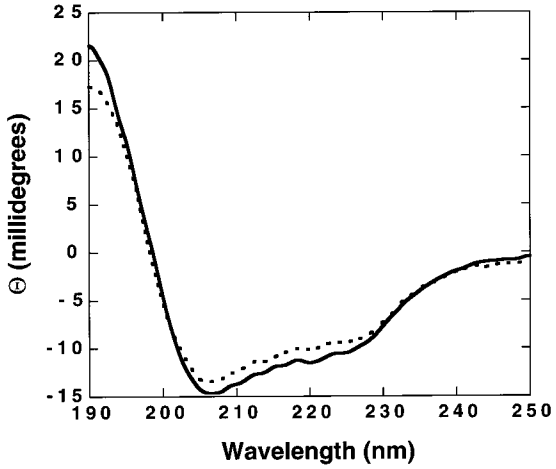

FIGURE 2: Circular dichroism spectra for 0.10 mM ZnFpg (solid line) and 0.088 mM CoFpg (dashed line) in 300 mM potassium phosphate (solid line), pH 7.2, 25 °C. The CD spectrum for CoFpg has been normalized relative to the concentration of ZnFpg.

0.5 mM, most of the duplex substrate is cleaved as indicated by the conversion of the band at the top of the gel to the cleavage product at the bottom of the gel (lanes 2 and 7). Progessively less substrate is cleaved with the addition of 10-fold dilutions of Fpg; however, cleavage is still observed at 0.0005 mM ZnFpg (lane 5) and 0.0005 mM CoFpg (lane 10). Note that the intensities of the bands are similar in the lanes containing equal concentrations of ZnFpg (lanes 2−5) and CoFpg (lanes 6−10). Together, these observations not only indicate that CoFpg is active, but also show that CoFpg is as active as ZnFpg.

Circular Dichroism Spectroscopy. The CD spectra for ZnFpg (solid curve) and CoFpg (dashed curve), shown in Figure 2, are similar and are characteristic of protein with substantial secondary structure. The double minima at 222 and 208−210 nm and the maximum between 190 and 195 nm suggest a significant amount of helical structure (*54*). CD spectra were also collected on the same sample after the addition of 10% glycerol to the solution (spectra not shown). Except for a small decrease in intensity due to dilution, the CD profiles for ZnFpg and CoFpg in 10% glycerol are identical to the CD profiles for the Fpg samples in the absence of glycerol. The latter observation indicates that 10% glycerol, at the limits of detection by CD spectroscopy, does not alter the solution structure of Fpg.

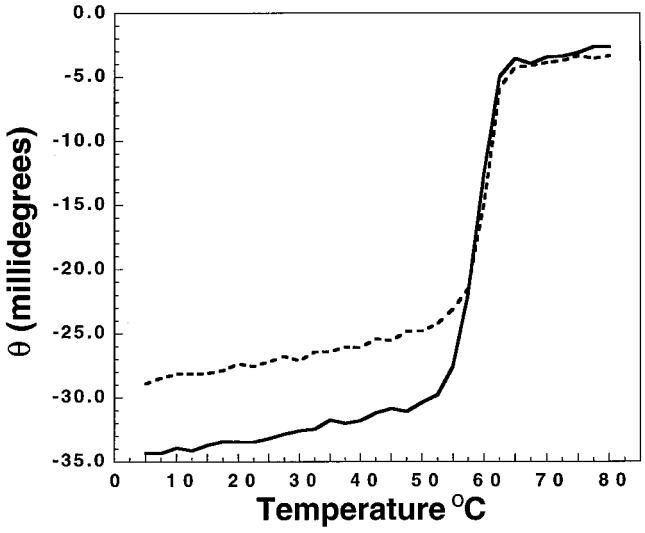

FIGURE 3: Thermal melts for 0.10 mM ZnFpg (solid line) and 0.088 mM CoFpg (dashed line). The data were collected at 220 nm in 2.5 °C intervals between 5 and 80 °C. The data have not been adjusted to reflect differences in protein concentrations.

Figure 3 shows the CD temperature melts for Zn- and CoFpg in NMR buffer measured at 220 nm. The measured ellipticities at low temperatures are not the same because the spectra have not been adjusted to reflect differences in protein concentration, approximately 12%. The measured ellipticities at high temperatures are the same because they represent a denatured, random coil structure for both samples. The CD melts for both proteins are similar with an inflection point at ∼60 °C, suggesting little, if any, difference in the stability between the zinc- and cobalt-associated Fpg. The sharp inflection point is characteristic of a cooperative transition between a structured and denatured state. Only a small rise is observed in the slope of the plot prior to the inflection point, suggesting little unraveling of individual domains or α-helices before denaturation (*56*). After cooling the Fpg samples back to 25 °C, the profiles of the CD spectra reflected a denatured protein (e.g., the ellipticity measured at 220 nm at 25 °C after heating was the same as that measured at 80 °C), indicating that denaturation was not reversible.

NMR Spectroscopy. Figure 4 is a two-dimensional ^{15}N/^{1}H HSQC spectrum of a 0.5 mM sample of ^{15}N-labeled ZnFpg that shows a wide chemical shift dispersion of the amide proton resonances (∼4 ppm) that is characteristic of a nonrandom protein conformation (*57*). The majority of the cross-peaks in the ^{15}N/^{1}H HSQC spectrum of CoFpg (Supporting Information, Figure 1) were in identical positions in the ^{15}N/^{1}H HSQC spectrum of ZnFpg, suggesting that the cobalt-associated protein was structurally similar to the zinc-associated protein. The cross-peaks in the CoFpg ^{15}N/^{1}H HSQC spectrum that were not in identical positions likely correspond to residues at, or near, the metal binding region of the protein. The resonances of such cross-peaks were likely shifted, or broadened beyond detection, due to the paramagnetic effect of Co^{2+} (*46*, *58*, *59*). The addition of

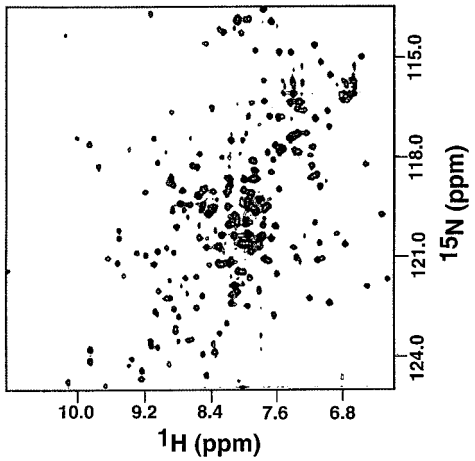

FIGURE 4: Two-dimensional ^{15}N/^{1}H HSQC-TROSY spectrum for ZnFpg in 300 mM potassium phosphate, 1 mM DTT, 10% D_2O/90% H_2O, pH 7.3, collected at a proton resonance frequency of 800 MHz.

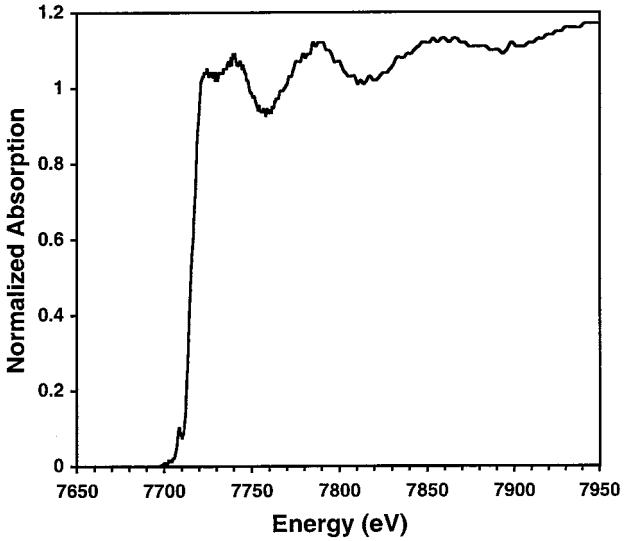

FIGURE 5: Cobalt K-edge XANES spectrum for lyophilized CoFpg (~77 K). The preedge feature at 7707 eV is the result of optical 1s-to-3d electronic transitions.

10% glycerol to the NMR samples of Fpg broadened the cross-peaks in the two-dimensional ^{15}N/^{1}H HSQC spectrum due, most likely, to an increase in viscosity (*60*). Otherwise, the chemical shifts of the amide proton and nitrogen resonances in the ^{15}N/^{1}H HSQC spectrum of Fpg in 10% glycerol were very similar to those in the spectrum collected in the absence of glycerol, suggesting that 10% glycerol had little, if any, effect on the solution structure of Fpg. Profiles of the two-dimensional ^{15}N/^{1}H HSQC of Fpg collected before and after lyophilization were also identical, suggesting that the metal was still properly coordinated to the protein in the lyophilized state. The only difference in the latter spectra was a loss in signal intensity (~15%) after lyophilization, suggesting that some of the protein aggregated or did not properly refold after redissolving in water.

At the NMR concentrations of ZnFpg, 0.5−0.7 mM, and in 300 mM phosphate buffer, the line widths of the cross-peaks in the ^{15}N/^{1}H HSQC spectra were ~40 Hz, a value in the range expected for a 30.2 kDa protein (*60*, *61*), suggesting the protein was monomeric in solution. A similar conclusion was reached with these protein concentrations by size exclusion chromatography (data not shown) and was previously observed by others at lower protein concentrations and under different buffer conditions (*10*, *62*).

EXAFS Spectroscopy. The X-ray absorption near-edge structure (XANES) spectra provide information to identify the metal, the metal valence, and the symmetry at the metal site as well as serving as a fingerprint for the local structure around the absorber. For example, with higher oxidation states, the absorption edge shifts to higher energy by a few eV, and for many transition elements with unfilled d orbitals, the shape of the XANES profile often reflects the geometry of the first coordination sphere. Figure 5 contains the XANES spectrum for lyophilized CoFpg and shows that the cobalt absorption edge energy, defined as the first inflection point, is 7714.3 eV for CoFpg, a value corresponding to a Co^{2+} oxidation state. Note that the cobalt edge for CoFpg in Figure 5 is not smooth, and a small preedge peak is observed at 7707.1 eV. The latter feature is assigned to a 1s-to-3d electronic transition and is sensitive to the symmetry of the ligands surrounding the Co^{2+} ion, following the same selection rules as for optical transitions (*42*). The observation of this preedge feature in CoFpg indicates that Co^{2+} is in a noncentrosymmetric environment because 1s-to-3d electronic transitions are dipole-forbidden. Therefore, the observed oscillator strength arises from p−d mixing, most likely at a site with tetrahedral symmetry. The absorption edge energy observed for ZnFpg in the lyophilized state is 9661.6 eV, a value corresponding to the Zn^{2+} oxidation state (Table 1). Unlike the XANES for CoFpg, the absorption edge for ZnFpg was smooth (no preedge features) because the d shell of Zn^{2+} is filled. Table 1 lists the main-edge and preedge absorption energies of the XANES spectra for CoFpg and ZnFpg in 10% aqueous glyercol and shows that they are similar to the values obtained for the two proteins in the lyophilized state. Therefore, the oxidation state of the metal in Fpg is the same in 10% frozen aqueous glycerol and in lyophilized form.

The EXAFS for ZnFpg and CoFpg in 10% frozen aqueous glycerol are compared in Figure 6 (jagged dark line). Analysis of the EXAFS oscillations provides quantitative information on the number and identity of atoms neighboring the absorber as well as information on the distance between the absorbing and neighboring atoms. The frequency of the EXAFS oscillations in the CoFpg spectrum is slightly lower than the frequency of the EXAFS oscillations in the ZnFpg spectrum, corresponding to a slightly shorter distance between absorber and nearest-neighbor atoms. In addition, there is a phase difference between the Zn and Co EXAFS oscillations that results from the difference in the absorber phase shift with Z and the arbitrary assignment of the ionization threshold, E_o. The EXAFS spectra for lyophilized ZnFpg and CoFpg were similar to the respective spectra obtained in 10% frozen aqueous glycerol illustrated in Figure 6.

The Fourier transforms of the EXAFS oscillations for Zn- and CoFpg, obtained in the lyophilized form and in 10% frozen aqueous glycerol, are compared in Figure 7. Note that the peaks in the Fourier transforms are uncorrected for phase shifts; therefore, they appear ~0.3 Å shorter than the actual distance from the absorber to the neighboring atoms. A single peak, at an almost identical radial distance, is observed in

Table 1: XANES Absorption Edge Energies and Fitting Results to the EXAFS Spectra for ZnFpg and CoFpg in 10% Frozen Aqueous Glycerol or Lyophilized (L)[a]

sample	main-edge (eV)	preedge (eV)	distance (Å)	number	sigma	r^2	ΔE_0
ZnFpg	9658.8	−	2.33 ± 0.01	3.5 ± 0.8	0.06 ± 0.01	1.3584	3.6 ± 3.0
ZnFpg (L)	9661.6	−	2.34 ± 0.01	4.1 ± 0.08	0.06 ± 0.01	0.9982	3.8 ± 2.2
CoFpg	7714.4	7707.3	2.28 ± 0.02	4.1 ± 1.1	0.07 ± 0.01	2.2165	0.8 ± 3.6
CoFpg (L)	7714.3	7707.2	2.29 ± 0.02	3.4 ± 0.8	0.06 ± 0.01	1.5061	2.9 ± 3.2
ZnS (L)	9659.0	−	2.33 ± 0.02	3.9 ± 0.7	0.04 ± 0.02	0.8893	−2.7 ± 2.4

[a] The uncertainties were determined as the quantity that a parameter could be varied from the value giving the best fit as to increase the r^2 value by 10% from its minimum value. The data for ZnS (L) are from Hess et al. (*46*).

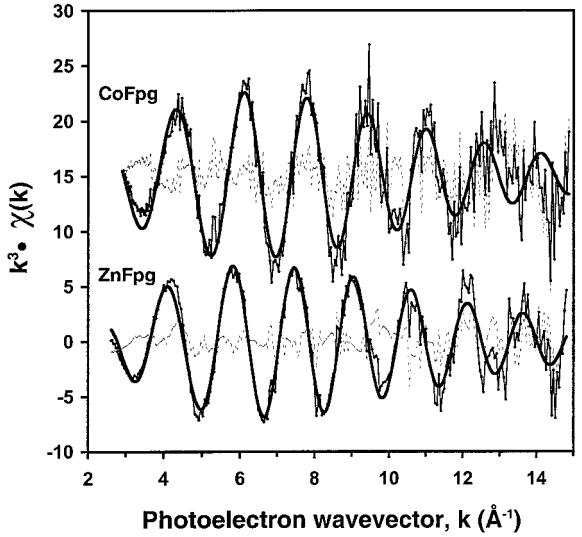

FIGURE 6: EXAFS spectra for ZnFpg and CoFpg in 10% frozen aqueous glycerol solution at ~77 K. The jagged dark line is the experimental data, the smooth dark line is the fit of the experimental data, and the dashed gray line is the subtraction of the experimental data from the fitted data.

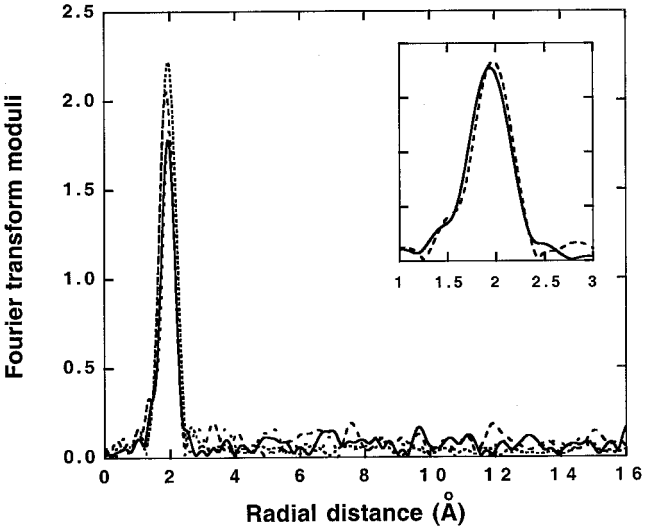

FIGURE 7: Fourier transforms of the ZnFpg and CoFpg EXAFS profiles over the photoelectron wavevector region from ~2 to 13 Å. The major peak in each of the Fourier transforms is due to sulfur atoms. There is extensive overlap of the spectra because the metal−sulfur bond lengths are all within 0.06 Å. The lyophilized spectra are the more intense peaks, ZnFpg (dotted) and CoFpg (dashed). The inset is an expansion of the EXAFS Fourier transforms for ZnFpg (solid) and CoFpg (dashed) in 10% frozen aqueous glycerol solution. All the peaks in the Fourier transforms are uncorrected for phase shifts and appear shorter than the actual distance from the absorber to the neighboring atoms.

the Fourier transforms of the EXAFS for all four samples. This major peak is due to the backscattering amplitude of sulfur atoms. While the metal−sulfur radial distance in all four samples is very similar, a close inspection of the data, illustrated in the inset of Figure 7 for ZnFpg and CoFpg in 10% frozen aqueous glycerol, indicates that the Co−S bond length is a few hundredths of an angstrom shorter than the Zn−S bond length. The same observation was made for the Fourier transforms of the EXAFS oscillation for lyophilized Zn- and Co-associated Fpg.

The EXAFS oscillations for ZnFpg and CoFpg were fit over the magnitude of the photoelectron wavevector region of 1.4−14.8 Å. Both proteins, in both states, are well fit by a single sulfur scattering wave. The goodness of fit is illustrated in Figure 6 where the fitting results (smooth dark line) for the samples in 10% aqueous glycerol are superimposed on their respective experimental data (jagged dark line). The dashed, light gray line in Figure 6 is the difference between the experimental data and fitting results and runs in the middle of both oscillations. Table 1 contains the fitting results for the four samples and shows that the metal in Zn- and CoFpg is coordinated to four sulfur atoms with an average metal−sulfur bond length that is 0.05 Å longer in the zinc-associated protein.

Proteins with zinc-binding motifs tetrahedrally coordinated to the sulfur atom of cysteine (C) residues and the nitrogen atom of one or two histidine (H) residues are common (*63*). The EXAFS spectra of proteins with such heteroresidue zinc-binding motifs are more complex due to the presence of a shorter (1.94 Å) zinc−nitrogen bond. As a consequence, such EXAFS profiles display multicomponent oscillations, and the corresponding Fourier transforms have extra peaks (*45*, *64*, *65*). Such differences are illustrated in Figure 8, a simulation of the EXAFS spectra (A) and the corresponding Fourier transforms (B) of all possible tetrahedral sulfur and nitrogen coordination to zinc. While the EXAFS oscillations for the C4 spectrum show a steady decay in amplitude, the C3N1 EXAFS oscillations contain a beat at approximately 7 $Å^{-1}$ in the decay which becomes progressively more pronounced in the C2N2 and C1N3 EXAFS oscillations (arrow in Figure 8A). Such a beat is not observed in the experimental EXAFS oscillations for ZnFpg or CoFpg (Figure 6). Furthermore, the Fourier transforms of the EXAFS oscillations containing the beat result in a peak to the left of the Zn−S peak that corresponds to a shorter Zn−N distance (arrow in Figure 8B). Such a peak was not observed in the Fourier transforms of the EXAFS data collected for ZnFpg and CoFpg (Figure 7). To make certain that such extra Zn−N shoulders in the Fpg EXAFS Fourier transforms would be observed if present, precautions in EXAFS data collection and analyses were taken (e.g.: $k_{max} > 13$ $Å^{-1}$, E_o was not varied, FEFF7.02) (*65*).

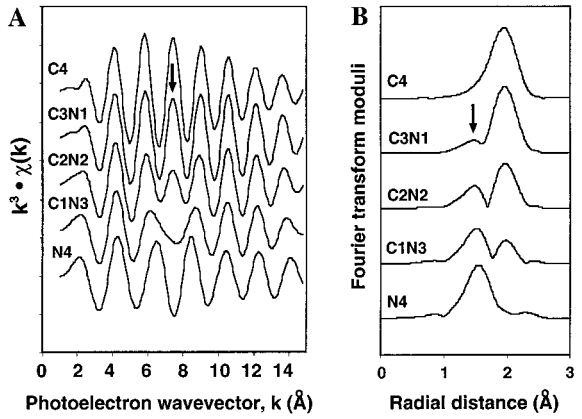

FIGURE 8: (A) Simulation of the EXAFS oscillations of all possible tetrahedral sulfur and nitrogen coordination to zinc: C4, C3N1, C2N2, C1N3, and N4. The arrow at $k = \sim 7$ Å^{-1} is a beat in the EXAFS amplitude due to Zn−N contributions. (B) Fourier transforms of the corresponding EXAFS oscillations. The arrow at a radial distance of ~1.5 Å is due to Zn−N contributions.

DISCUSSION

Characterization of the Fpg EXAFS Samples. The DNA glycosylase activity of Fpg is not altered upon the substitution of Zn^{2+} with Co^{2+}, implying that the structures of ZnFpg and CoFpg are also not altered. Similar CD and NMR spectra for zinc- and cobalt-associated Fpg corroborate such a conclusion. Furthermore, the CD and NMR spectra collected for ZnFpg and CoFpg in the presence of 10% glycerol were similar to the respective spectra obtained in the absence of glycerol. Such a result indicates that 10% glycerol had little, if any, effect on the structures of Fpg. The NMR data and size exclusion chromatography also showed that both ZnFpg and CoFpg are monomeric in solution. Circular dichroism temperature melts showed that substitution of Zn^{2+} with Co^{2+} did not alter the stability of Fpg. Taken together, the DNA glycosylase assay and the CD and NMR data show that prior to lyophilization or freezing in 10% aqueous glycerol, the Fpg preparations used for the EXAFS experiments were monomeric in solution, structured, and active.

Identification of a C4-Type Metal-Binding Domain in Fpg. The EXAFS experiments showed that the metal in Fpg was coordinated to the sulfur atom of four cysteine residues. The 2.33 Å zinc−sulfur bond length observed for the metal center in ZnFpg is almost identical to the EXAFS-determined Zn−S bond length obtained for other C4-type metalloproteins. A 2.34 Å Zn−S bond length was observed in the *E. coli* UvrA protein, a damage recognition subunit of ABC excision nuclease (*43*). A 2.34 Å Zn−S bond length was also observed in the minimal DNA binding domain of human XPA (*46*) and in full-length *Xenopus laevis* XPA (*66*). XPA is a protein crucial to nucleotide excision repair (*67*). While Co^{2+} has been substituted for Zn^{2+} in a number of metalloproteins (*58*), the only EXAFS study of a C4-type, cobalt-associated protein is on the minimal DNA binding domain of XPA (*46, 68*). In the latter studies of XPA, a Co−S bond length of 2.34 Å was observed. The 2.28 Å Co−S bond length reported here for CoFpg is 0.06 Å shorter than that observed for XPA, suggesting that the metal-binding domain is slightly more compact in CoFpg than it is in ZnFpg and XPA. However, relative to ZnFpg, the slightly shorter metal bond length in CoFpg had no detectable effect on the DNA glycosylase activity of Fpg (Figure 1). As observed for UvrA and XPA, the EXAFS data for Zn- and CoFpg contain no evidence to indicate that the metal is coordinated to the imidazole nitrogen of a histidine residue.

The EXAFS data indicate that Zn^{2+} and Co^{2+} metal ions have associated with ZnFpg and CoFpg, respectively. The association of one molecule of Zn^{2+} per molecule of Fpg protein has previously been shown by atomic absorption spectroscopy (*62*). The data presented here are the first direct evidence for the association of Co^{2+} with Fpg. In addition to verifying the metal association with Fpg, the EXAFS data provide direct evidence that the metal in Fpg is coordinated to the sulfur atom of four cysteine residues. However, there are six cysteine residues in Fpg (C147, C195, C244, C247, C264, and C267), and EXAFS data alone cannot distinguish which cysteine residues are involved in chelating the metal. A substantial body of indirect evidence strongly suggests that the four C-terminal cysteine residues are involved in metal chelation. Primary amino acid sequence analysis of Fpg for secondary structure identifies a C4-type metal-binding motif involving the four C-terminal cysteine residues (*39*). Individual site-directed mutatgenesis of each of the six cysteine residues to a glycine showed only minor changes in the activities of Fpg for the C147G and C195G mutations, but dramatic effects on the activities of Fpg for the C244G, C247G, C264G, and C267G mutations (*40*). A double amino acid substitution of two of the four C-terminal cysteine residues to serine, C244S/C247S, resulted in a protein with no DNA binding or cleavage activity and that did not bind zinc (*10*).

Cobalt(II) as a Paramagnetic Probe of the Structure of Fpg. The zinc-binding motif in Fpg plays a critical role in recognizing and binding to damaged DNA (*10, 40*). While the protein scaffold for DNA binding is located at the C-terminus of Fpg, the catalytic site of the DNA glycosylase and AP lyase activities of Fpg are at the N-terminus (*69, 70*). Consequently, the structural basis for damaged DNA recognition and the catalytic activities of Fpg promise to be very interesting. Efforts are currently in progress, using ^{13}C- and ^{15}N-labeled Fpg samples, to determine the solution structure of Fpg. Valuable to those efforts will be the substitution of diamagnetic Zn^{2+} with paramagnetic Co^{2+} (*59, 71*). Pseudocontact shifts, mediated by dipolar (through space) interaction of Co^{2+} with neighboring nuclei, have a $1/r^3$ distance dependence (*59*). Such an interaction contains distance information that extends up to 20 Å from the metal site, unlike proton−proton NOEs that have a $1/r^6$ distance dependence and contain distance information that extends only out to 5−7 Å. The EXAFS data presented here unambiguously show that it is possible to substitute Zn^{2+} with Co^{2+} in the metal center of Fpg with only minor differences in the average metal−sulfur bond distances. Furthermore, CD and two-dimensional $^{15}N/^{1}H$ HSQC spectra suggest that the structures of ZnFpg and CoFpg are similar, and the 8-oxoG cleavage assay shows that the activity of ZnFpg is indistinguishable from CoFpg. Therefore, NMR experiments with CoFpg should be biologically relevant.

ACKNOWLEDGMENT

We thank Dr. Steven D. Conradson for the use of equipment essential for EXAFS data collection and for providing his software for data analysis.

SUPPORTING INFORMATION AVAILABLE

A figure containing the $^{15}N/^{1}H$ HSQC spectrum of CoFpg (1 page). This material is available free of charge via the Internet at http://pubs.acs.org.

REFERENCES

1. Tchou, J., Kasai, H., Shibutani, S., Chung, M. H., Laval, J., Grollman, A. P., and Nishimura, S. (1991) *Proc. Natl. Acad. Sci. U.S.A. 88*, 4690−4694.
2. Friedberg, E. C., Walker, G. C., and Siede, W. (1995) in *DNA Repair and Mutagenesis*, pp 158−161, American Society for Microbiology, Washington, DC.
3. Adelman, R., Saul, R. L., and Ames, B. N. (1988) *Proc. Natl. Acad. Sci. U.S.A. 85*, 2706−2708.
4. Lindahl, T. (1993) *Nature 362*, 709−715.
5. Cleaver, J. E., and Kraemer, K. H. (1989) in *The Metabolic Basis of Inherited Disease* (Scriver, S. C., Beaudet, A. L., Sly, W. S., and Valle, D., Eds.) McGraw-Hill Book Co., New York.
6. Wallace, S. S. (1997) in *Oxidative Stress and the Molecular Biology of Antioxidant Defenses*, pp 49−90, Cold Spring Harbor Press, Cold Spring Harbor, NY.
7. David, S. S., and Williams, S. D. (1998) *Chem. Rev. 98*, 1221−1261.
8. McCullough, A. K., Dodson, M. L., and Lloyd, R. S. (1999) *Annu. Rev. Biochem. 68*, 255−285.
9. Boiteux, S., O'Connor, T. R., and Laval, J. (1987) *EMBO J. 6*, 3177−3183.
10. Tchou, J., Michaels, M. L., Miller, J. H., and Grollman, A. P. (1993) *J. Biol. Chem. 268*, 26738−26744.
11. Boiteux, S., Gajewski, E., Laval, J., and Dizdaroglu, M. (1992) *Biochemistry 31*, 106−110.
12. Chetsanga, C. J., and Lindhal, T. (1979) *Nucleic Acids Res. 6*, 3673−3684.
13. Duarte, V., Gasparutto, D., Jaquinod, M., and Cadet, J. (2000) *Nucleic Acids Res. 28*, 1555−1563.
14. Hatahet, Z., Kow, Y. W., Purmal, A. A., Cunningham, R. P., and Wallace, S. S. (1994) *J. Biol. Chem. 269*, 581−589.
15. D'Ham, C., Romieu, A., Jaquinod, M., Gasparutto, D., and Cadet, J. (1999) *Biochemistry 38*, 3335−3344.
16. Jurado, J., Saparbaev, M., Matray, M. J., Greenberg, M. M., and Laval, J. (1998) *Biochemistry 37*, 7757−7763.
17. Bailly, V., Verly, W. G., O'Connor, T., and Laval, J. (1989) *Biochem. J. 262*, 581−589.
18. O'Connor, T. R., and Laval, J. (1989) *Proc. Natl. Acad. Sci. U.S.A. 86*, 5222−5226.
19. Bhagwat, M., and Gerlt, J. A. (1996) *Biochemistry 35*, 659−665.
20. Graves, R. J., Felzenszwalb, J., Laval, J., and O'Connor, T. (1992) *J. Biol. Chem. 267*, 14429−14435.
21. Cabrera, M., Nghiem, Y., and Miller, J. H. (1988) *J. Bacteriol. 170*, 5405−5407.
22. Michaels, M. L., Cruz, C., Grollman, A. P., and Miller, J. H. (1992) *Proc. Natl. Acad. Sci. U.S.A. 89*, 7022−7025.
23. Shibutani, M., Takeshita, M., and Grollman, A. P. (1991) *Nature 349*, 431−434.
24. Wood, M. L., Dizdaroglu, M., Gajewski, E., and Essigmann, J. M. (1990) *Biochemistry 29*, 7024−7032.
25. Moriya, M., Ou, C., Bodepudi, V., Johnson, F., Takeshita, M., and Grollman, A. P. (1991) *Mutat. Res. 254*, 281−288.
26. Cheng, K. C., Cahill, D. S., Kasai, H., Nishimura, S., and Loeb, L. A. (1992) *J. Biol. Chem. 267*, 166−172.
27. Moriya, M. (1993) *Proc. Natl. Acad. Sci. U.S.A. 90*, 1122−1126.
28. Moriya, M., and Grollman, A. P. (1993) *Mol. Gen. Genet. 239*, 72−76.
29. Lu, A.-L., and Chang, D.-Y. (1988) *Cell 54*, 805−812.
30. Au, K. G., Clark, S., Miller, J. H., and Modrich, P. (1989) *Proc. Natl. Acad. Sci. U.S.A. 86*, 8877−8881.
31. Tsai-Wu, J. J., Liu, H. F., and Lu, A. L. (1992) *Proc. Natl. Acad. Sci. U.S.A. 89*, 8779−8783.
32. Auffret van der Kemp, P., Thomas, D., Barbey, R., de Oliveira, R., and Boiteux, S. (1996) *Proc. Natl. Acad. Sci. U.S.A. 93*, 5197−5202.
33. Arai, K., Morishita, K., Shinmura, K., Kohno, T., Kim, S.-R., Nohmi, T., Taniwaki, S., Ohwada, S., and Yokota, J. (1997) *Oncogene 14*, 2857−2861.
34. Aburatani, H., Hippo, Y., Ishida, T., Takashima, R., Matsuba, C., Kodama, T., Takao, M., Yasui, A., Yamamoto, K., Asano, M., Fukasawa, K., Yoshinari, T., Inoue, H., Ohtsuka, E., and Nishimura, S. (1997) *Cancer Res. 57*, 2151−2156.
35. Radicella, J. P., Dherin, C., Desmaze, C., Fox, M. S., and Boiteux, S. (1997) *Proc. Natl. Acad. Sci. U.S.A. 94*, 8010−8015.
36. Roldán-Arjona, T., Wei, Y.-F., Carter, K. C., Klungland, A., Anselmino, C., Wang, R.-P., Augustus, M., and Lindahl, T. (1997) *Proc. Natl. Acad. Sci. U.S.A. 94*, 8016−8020.
37. Bjørås, M., Luna, L., Johnsen, B., Hoff, E., Haug, T., Rognes, T., and Seeberg, E. (1997) *EMBO J. 16*, 6314−6322.
38. Rosenquist, T. A., Zharkov, D. O., and Grollman, A. P. (1997) *Proc. Natl. Acad. Sci. U.S.A. 94*, 7429−7434.
39. Grollman, A. P. (1992) in *Proceedings of the Seventh Conversation in Biomolecular Stereodynamics* (Sarma, R. H., and Sarma, M. H., Eds.) pp 165−170, Adenine Press, New York.
40. O'Connor, T. R., Graves, R. J., de Murcia, G., Castaing, B., and Laval, J. (1993) *J. Biol. Chem. 268*, 9063−9070.
41. Teo, B. K. (1981) in *EXAFS Spectroscopy: Techniques and Applications* (Teo, B. K., and Joy, D. C., Eds.) pp 13−58, Plenum Publishing Corp., New York.
42. Brown, G. E., Jr., Calas, G., Waychunas, G. A., and Petiau, J. (1988) *Rev. Mineral. 18*, 431−512.
43. Navaratnam, S., Myles, G. M., Strange, R. W., and Sancar, A. (1989) *J. Biol. Chem. 264*, 16067−16071.
44. Summers, M. F., Henderson, L. E., Chance, M. R., Bess, J. W., Jr., South, T. L., Blake, P. R., Sagi, I., Perez-Alvarado, G., Sowder, R. C., III, Hare, D. R., and Arthur, L. O. (1992) *Protein Sci. 1*, 563−574.
45. Strange, R. W., Murphy, L. M., Karlsson, B. G., Reinhammar, B., and Hasnain, S. S. (1996) *Biochemistry 35*, 16391−16398.
46. Hess, N. J., Buchko, G. W., Conradson, S. D., Espinosa, F. J., Ni, S., Thrall, B. D., and Kennedy, M. A. (1998) *Protein Sci. 7*, 1970−1975.
47. Bertini, I., and Luchinat, C. (1984) in *Advances in Inorganic Biochemistry* (Eichorn, G. L., and Marzilli, L. G., Eds.) pp 71−111, Elsevier, New York.
48. Kay, L. E., Keifer, P., and Saarinen, T. (1992) *J. Am. Chem. Soc. 114*, 10663−10665.
49. Zhang, O., Kay, L. E., Olivier, J. P., and Forman-Kay, J. D. (1994) *J. Biol. NMR 4*, 845−858.
50. Pervushin, K., Riek, R., Wider, G., and Wüthrich, K. (1997) *Proc. Natl. Acad. Sci. U.S.A. 94*, 12366−12371.
51. McMaster, W. H., Kerr del Grande, N., Mallett, J. H., and Hubbell, J. H. (1969) in *Compilation of X-ray cross sections*, p 350, University of California, Livermore, CA.
52. Rehr, J. J., Mustre de Leon, J., Zabinsky, S. I., and Albers, R. C. (1991) *J. Am. Chem. Soc. 113*, 5135−5140.
53. Ankudinov, A. L. (1996) in Ph.D. Thesis, *Self-energy models in XAFS, XANES and XMCD*, University of Washington, Seattle, WA.
54. Holzwarth, G. M., and Doty, P. (1965) *J. Am. Chem. Soc. 87*, 218−228.
55. Rizo, J., Blanco, F. J., Kobe, B., Bruch, M. D., and Gierasch, L. M. (1993) *Biochemistry 32*, 4881−4894.
56. Creigton, T. E. (1993) in *Proteins: Structure and Molecular Properties*, pp 287−291, W. H. Freeman, New York.
57. Muhandiram, D. R., and Kay, L. E. (1994) *J. Magn. Reson. B 103*, 203−216.
58. Donaire, A., Salgado, J., Jimenez, H. R., and Moratal, J. M. (1995) in *Nuclear Magnetic Resonance of Paramagnetic Macromolecules* (La Mer, G. N., Ed.) pp 213−244, Kluwer Academic Publishers, Dordrecht, The Netherlands.

59. Gochin, M., and Roder, H. (1995) *Protein Sci. 4*, 296−305.
60. Cavanagh, J., Fairbrother, W. J., Palmer, A. G., III, and Skelton, N. J. (1996) in *Protein NMR Spectroscopy. Principles and Practice*, pp 16−19, Academic Press, Inc., San Diego, CA.
61. Lee, A. L., Volkman, B. F., Robertson, S. A., Rudner, D. Z., Barbash, D. A., Cline, T. W., Kanaar, R., Rio, D. C., and Wemmer, D. E. (1997) *Biochemistry 36*, 14306−14317.
62. Boiteux, S., O'Connor, T. R., Lederer, F., Gouyette, A., and Laval, J. (1990) *J. Biol. Chem. 265*, 3916−3922.
63. Berg, J. M., and Shi, Y. (1996) *Science 271*, 1081−1086.
64. Zhang, K., and Auld, D. S. (1995) *Biochemistry 34*, 16306−16312.
65. Clark-Baldwin, K., Tierney, D. L., Nandakumar, G., Gruff, E. S., Kim, C., Berg, J., Koch, S. A., and Penner-Hahn, J. E. (1998) *J. Am. Chem. Soc. 120*, 8401−8409.
66. Buchko, G. W., Iakoucheva, L. M., Kennedy, M. A., Ackerman, E. J., and Hess, N. J. (1999) *Biochem. Biophys. Res. Commun. 254*, 109−113.
67. Wood, R. D. (1997) *J. Biol. Chem. 272*, 777−791.
68. Buchko, G. W., Hess, N. J., and Kennedy, M. A. (2000) *Protein Pept. Lett. 7*, 49−56.
69. Zharkov, D. O., Rieger, R. A., Iden, C. R., and Grollman, A. P. (1997) *J. Biol. Chem. 272*, 5335−5241.
70. Sidorkina, O. M., and Laval, J. (2000) *J. Biol. Chem. 275*, 9924−9929.
71. Buchko, G. W., Daughdrill, G. W., de Lorimier, R., Rao, S. B. K., Isern, N. G., Lingbeck, J., Taylor, J.-S., Wold, M. S., Gochin, M., Spicer, L. D., Lowry, D. F., and Kennedy, M. A. (1999) *Biochemistry 38*, 15116−15128.

BI001377K